Early-Phase ^{18}F-Florbetapir and ^{18}F-Flutemetamol Images as Proxies of Brain Metabolism in a Memory Clinic Setting

Cecilia Boccalini[1–3], Débora Elisa Peretti[1], Federica Ribaldi[4,5], Max Scheffler[6], Sara Stampacchia[1], Szymon Tomczyk[4], Cristelle Rodriguez[7,8], Marie-Louise Montandon[8,9], Sven Haller[10–13], Panteleimon Giannakopoulos[7,8], Giovanni B. Frisoni[4,5], Daniela Perani[2,3,14], and Valentina Garibotto[1,15,16]

[1]Laboratory of Neuroimaging and Innovative Molecular Tracers (NIMTlab), Geneva University Neurocenter and Faculty of Medicine, University of Geneva, Geneva, Switzerland; [2]Vita-Salute San Raffaele University, Milan, Italy; [3]In Vivo Human Molecular and Structural Neuroimaging Unit, Division of Neuroscience, IRCCS San Raffaele Scientific Institute, Milan, Italy; [4]Laboratory of Neuroimaging of Aging (LANVIE), University of Geneva, Geneva, Switzerland; [5]Memory Clinic, Geneva University Hospitals, Geneva, Switzerland; [6]Division of Radiology, Diagnostic Department, Geneva University Hospitals, Geneva, Switzerland; [7]Division of Institutional Measures, Medical Direction, University Hospitals of Geneva, Geneva, Switzerland; [8]Department of Psychiatry, Faculty of Medicine, University of Geneva, Geneva, Switzerland; [9]Department of Rehabilitation and Geriatrics, Geneva University Hospitals and University of Geneva, Geneva, Switzerland; [10]CIMC–Centre d'Imagerie Médicale de Cornavin, Geneva, Switzerland; [11]Faculty of Medicine of University of Geneva, Geneva, Switzerland; [12]Division of Radiology, Department of Surgical Sciences, Uppsala University, Uppsala, Sweden; [13]Department of Radiology, Beijing Tiantan Hospital, Capital Medical University, Beijing, China; [14]Nuclear Medicine Unit, San Raffaele Hospital, Milan, Italy; [15]Division of Nuclear Medicine and Molecular Imaging, Geneva University Hospitals, Geneva, Switzerland; and [16]CIBM Center for Biomedical Imaging, Geneva, Switzerland

Alzheimer disease (AD) neuropathologic changes are β-amyloid (Aβ) deposition, pathologic tau, and neurodegeneration. Dual-phase amyloid PET might be able to evaluate Aβ deposition and neurodegeneration with a single tracer injection. Early-phase amyloid PET scans provide a proxy for cerebral perfusion, which has shown good correlations with neural dysfunction measured through metabolic consumption, whereas the late frames depict amyloid distribution. Our study aimed to assess the comparability between early-phase amyloid PET scans and ^{18}F-FDG PET brain topography at the individual level and their ability to discriminate patients. **Methods:** One hundred sixty-six subjects evaluated at the Geneva Memory Center, ranging from no cognitive impairment to mild cognitive impairment and dementia, underwent early-phase amyloid PET—using either ^{18}F-florbetapir (eFBP) ($n = 94$) or ^{18}F-flutemetamol (eFMM) ($n = 72$)—and ^{18}F-FDG PET. Aβ status was assessed. SUV ratios (SUVRs) were extracted to evaluate the correlation of eFBP/eFMM and their respective ^{18}F-FDG PET scans. The single-subject procedure was applied to investigate hypometabolism and hypoperfusion maps and their spatial overlap by the Dice coefficient. Receiver-operating-characteristic analyses were performed to compare the discriminative power of eFBP/eFMM and ^{18}F-FDG PET SUVR in AD-related meta–regions of interest between Aβ-negative healthy controls and cases in the AD continuum. **Results:** Positive correlations were found between eFBP/eFMM and ^{18}F-FDG PET SUVR independently of Aβ status and Aβ radiotracer ($R > 0.72$, $P < 0.001$). eFBP/eFMM single-subject analysis revealed clusters of significant hypoperfusion with good correspondence to hypometabolism topographies, independently of the underlying neurodegenerative patterns. Both eFBP/eFMM and ^{18}F-FDG PET SUVR significantly discriminated AD patients from controls in the AD-related meta–regions of interest (eFBP area under the curve [AUC], 0.888; eFMM AUC, 0.801), with ^{18}F-FDG PET performing slightly better, although not significantly (all P values higher than 0.05), than others (^{18}F-FDG AUC, 0.915 and 0.832 for subjects evaluated with eFBP and eFMM, respectively). **Conclusion:** The distribution of perfusion was comparable to that of metabolism at the single-subject level by parametric analysis, particularly in the presence of a high neurodegeneration burden. Our findings indicate that eFBP and eFMM imaging can replace ^{18}F-FDG PET imaging, as they reveal typical neurodegenerative patterns or allow exclusion of the presence of neurodegeneration. The findings show cost-saving capacities of amyloid PET and support routine use of the modality for individual classification in clinical practice.

Key Words: neurodegeneration; early-phase amyloid PET; ^{18}F-FDG PET; individual maps

J Nucl Med 2023; 64:266–273
DOI: 10.2967/jnumed.122.264256

PET can provide in vivo evaluation of protein deposition and neuronal injury (*1*), playing a leading role in the diagnosis of Alzheimer disease (AD) and other dementia conditions. Brain ^{18}F-FDG PET is a well-established tool for investigating neurodegeneration, through the detection of changes in cerebral glucose metabolism. Regional analysis of the ^{18}F-FDG PET signal can reveal specific brain hypometabolism patterns highly indicative of neurodegeneration along the AD, frontotemporal dementia, and Lewy body spectrum, including subjects from the preclinical phases to clinically overt dementia (*2*). In longitudinal studies, the absence of disease-specific hypometabolism patterns was a strong predictor of preserved cognition (*3–5*).

Amyloid PET imaging, initially with ^{11}C-labeled Pittsburgh compound B and now also with 3 ^{18}F-labeled compounds, namely ^{18}F-florbetapir, ^{18}F-florbetaben, and ^{18}F-flutemetamol, allows the assessment of β-amyloid (Aβ) plaque burden in vivo (*1*). A dual-phase amyloid PET protocol of acquisition has been proposed, adding to the reference late acquisition an acquisition of the tracer distribution immediately after injection (*6*). These early-phase images can

Received Apr. 8, 2022; revision accepted Jul. 15, 2022.
For correspondence or reprints, contact Cecilia Boccalini (cecilia.boccalini@unige.ch).
Published online Jul. 21, 2022.

provide a proxy for cerebral perfusion because of the high lipophilicity of the tracers (*6,7*). In turn, cerebral perfusion is strongly related to neural dysfunction as measured through metabolic consumption (*8,9*). In AD, the early-phase acquisition of amyloid PET has shown a good correlation to ^{18}F-FDG PET uptake at the group level, suggesting its potential use as a biomarker of neuronal dysfunction (*10–21*).

Despite multiple descriptions in the literature of dual-phase amyloid PET, the use of early-phase images in clinical and research settings is not yet widely implemented. Our study explored the utility of early-phase images of amyloid PET scans, using either ^{18}F-florbetapir or ^{18}F-flutemetamol, for individual classification and their comparability with the respective ^{18}F-FDG PET brain hypometabolic voxel-wise maps in a memory clinic cohort.

MATERIALS AND METHODS

Participants

The study included subjects assessed at the Geneva University Hospitals, ranging from cognitively unimpaired (CU) to mild cognitive impairment (MCI) and dementia, in 2 ongoing studies as described previously (*22–26*). The local ethics committee approved the different imaging studies, which were conducted under the principles of the Declaration of Helsinki and the International Conference on Harmonization good clinical practice. The requirement to obtain informed consent was waived.

We included a total of 166 subjects classified as Aβ-negative (Aβ−) CU ($n = 42$), Aβ-positive (Aβ+) CU ($n = 30$), MCI ($n = 73$) (*27*), and dementia ($n = 21$) (*28*) subjects, following standardized criteria for clinical staging. Specifically, the Aβ− CU group, including healthy volunteers and individuals with subjective cognitive decline (*29*), all with ^{18}F-FDG PET–negative scans, was used as a healthy control (HC) reference for comparisons. The Aβ+ CU group was considered a group of interest, given the higher risk of progression in this population (*30*). Inclusion criteria were at least one 3-dimensional T1-weighted MRI scan, dual-phase amyloid PET using either ^{18}F-florbetapir or ^{18}F-flutemetamol, an ^{18}F-FDG PET scan, and an interval of less than 1 year between imaging measures.

MRI Acquisition

MRI was performed at Geneva University Hospitals' Division of Radiology using a 3-T scanner (Magnetom Skyra; Siemens Healthineers) equipped with a 20- or 64-channel head coil. The supplemental materials, section 1, detail the acquisition parameters (supplemental materials are available at http://jnm.snmjournals.org). The lesion prediction algorithm (*31*), implemented in the lesion segmentation toolbox, was used to segment fluid-attenuated inversion recovery images, allowing us to extract the total lesion volume. White matter lesions were also quantified visually according to the age-related white matter change scale (*32*).

PET Acquisition

^{18}F-FDG PET and amyloid PET were performed at the Division of Nuclear Medicine and Molecular Imaging at Geneva University Hospitals using a Biograph 128 mCT, Biograph 128 Vision 600 Edge, Biograph 40 mCT, or Biograph 64 TruePoint PET scanner (Siemens Medical Solutions). All scanners were comparable. ^{18}F-FDG PET was performed according to the European Association of Nuclear Medicine guidelines (*33,34*). Amyloid PET images were acquired using ^{18}F-florbetapir (FBP) ($n = 94$) or ^{18}F-flutemetamol (FMM) ($n = 72$). Amyloid status (Aβ+/Aβ−) was determined for each late image by an expert in nuclear medicine, applying the standard operating procedures approved by the European Medicines Agency.

Regarding the early phase of amyloid PET (eFBP and eFMM), the image acquisition was started immediately after tracer injection, and a static image was acquired for 5 min (eFBP) or 10 min (eFMM) (*20,35*).

The supplemental materials, section 2, provide full details on the PET acquisition.

MRI and PET Normalization Processing

Processing was performed as previously described (*25*) using Statistical Parametric Mapping (SPM 12; Wellcome Trust Centre for Neuroimaging), running in MATLAB R2018b, version 9.5 (MathWorks Inc.). All details are reported in the supplemental materials, section 3.

SUV Ratio (SUVR) Extraction in Automated Anatomic Labeling (AAL) ROIs and AD Meta–Region of Interest (Meta-ROI)

Uptake values were extracted within regions from AAL atlas 3 (*36*) and key regions sensitive to AD according to a predefined meta-ROI approach (*37*). SUVRs were calculated by normalizing the uptake to the mean value of the pons and cerebellar vermis together as the reference region. Intensity-normalized PET images were saved for further voxelwise analyses.

Single-Subject Voxel-wise Analyses

According to a validated SPM single-subject procedure (*38*), each PET image was tested for relative hypometabolism/hypoperfusion by means of a 2-sample *t* test in comparison with PET images of controls. HC groups included 28 and 14 subjects with Aβ− and ^{18}F-FDG PET–negative scans, for eFBP and eFMM samples, respectively. We used the same HC subjects also for the ^{18}F-FDG PET analyses. The statistical threshold for the resulting hypometabolic and hypoperfusion SPM maps was set at a P value of 0.05, uncorrected for multiple comparisons, considering significant clusters containing more than 100 voxels. SPM maps were then binarized for further Dice analyses. The resulting single-subject SPM hypometabolic maps were visually inspected by nuclear medicine experts blinded to clinical diagnoses and classified into hypometabolism patterns suggestive of neurodegenerative conditions (*3,39–41*) or excluding the presence of neurodegeneration. Hypometabolic and hypoperfusion maps were visually inspected at the single-subject level to define the visual match between maps. The same assessment was applied also to ^{18}F-FDG PET and eFBP/eFMM uptake distribution images.

Statistical Analysis

Dice coefficients were calculated, using FSL software (*42*), to quantify the whole-brain spatial overlap between hypometabolic and hypoperfusion binary maps at the single-subject level (supplemental materials, section 4) (*43*). Moreover, we calculated Δ scores between the hypometabolic and hypoperfusion maps' extents (number of voxels) to quantify discrepancies between the 2 patterns.

General linear models were performed to assess the correlation between eFBP/eFMM SUVR in the AAL ROIs and their respective ^{18}F-FDG SUVR in the whole sample. We assessed the correlations also in Aβ+ and Aβ− subjects separately. We tested the correlation of eFBP, eFMM, and ^{18}F-FDG SUVR in the AD composite meta-ROI with Mini-Mental State Examination scores.

Finally, we identified patients in the AD continuum, including specifically MCI and AD dementia cases according to the Aβ+ status and AD-like hypometabolism patterns. We performed receiver-operating-characteristic (ROC) analyses to compare the discriminative power of eFBP, eFMM, and ^{18}F-FDG meta-ROI SUVRs between HC and AD patients. The resulting areas under the curve (AUCs) from different tracers were compared using a De Long test (*44*) for 2 correlated ROC curves, setting the threshold for significance at a P value of 0.05. All statistical analyses were performed with R, version 4.0.2 (R Foundation for statistical computing, https://www.r-project.org/).

TABLE 1
Demographic Characteristics of Subjects

Characteristic	Whole sample	FBP group	FMM group	*P**
n	166	94	72	
Age	73.18 ± 6.35	74.27 ± 5.548	71.76 ± 7.068	0.012
Sex				0.425
Female	98	58	40	
Male	68	36	32	
MMSE	25.92 ± 4.00	26.12 ± 3.857	25.66 ± 4.202	0.471
Aβ status				0.980
Negative	70	39	31	
Positive	93	52	41	
Clinical groups according to Aβ status				
Aβ+ AD dementia	18	13	5	
Aβ− dementia	3	2	1	
Aβ+ MCI	52	31	22	
Aβ− MCI	21	9	11	
Aβ+ CU	30	11	19	
Aβ− CU (HC)	42	28	14	

*From *t* test comparing data from eFBP and eFMM subgroups.
MMSE = Mini-Mental State Examination; FBP = florbetapir; FMM = flutemetamol; *n* = number; Aβ− = amyloid negative; Aβ+ = amyloid positive; AD = Alzheimer disease; MCI = mild cognitive impairment; CU = cognitively unimpaired; HC = healthy controls.
Qualitative data are number; continuous data are mean ± SD.

RESULTS

Demographic and clinical data for our cohort are displayed in Table 1. The average intervals between amyloid PET and ^{18}F-FDG PET, between MRI and ^{18}F-FDG PET, and between MRI and amyloid PET were 2.15 months (SD, 3.06), 1.89 months (SD, 4.15), and 2.76 months (SD, 3.40), respectively.

Correlations Between eFBP/eFMM and ^{18}F-FDG SUVR

Both eFBP and eFMM SUVR in the AAL ROIs presented a strong correlation with ^{18}F-FDG SUVR in the whole group (eFBP $r = 0.786$, $P < 0.001$; eFMM $r = 0.806$, $P < 0.001$). Good correlations between eFBP/eFMM and ^{18}F-FDG SUVR were also found separately in Aβ+ (eFBP $r = 0.843$, $P < 0.001$; eFMM $r = 0.827$, $P < 0.001$) and Aβ− (eFBP $r = 0.72$, $P < 0.001$; eFMM $r = 0.791$, $P < 0.001$) subjects. Figure 1 shows scatterplots for the whole sample and subgroups according to Aβ status.

The composite meta-ROI SUVRs for eFBP/eFMM uptake and those for ^{18}F-FDG uptake correlated significantly with Mini-Mental State Examination scores (^{18}F-FDG $r = 0.536$, $P < 0.001$; eFBP $r = 0.413$, $P < 0.001$; eFMM $r = 0.482$, $P < 0.001$).

Single-Subject eFBP/eFMM and ^{18}F-FDG Patterns

The SPM single-subject analysis revealed disease-specific hypometabolism and hypoperfusion maps (Fig. 2; Tables 2 and 3). The supplemental materials, section 5, and Supplemental Tables 1–3

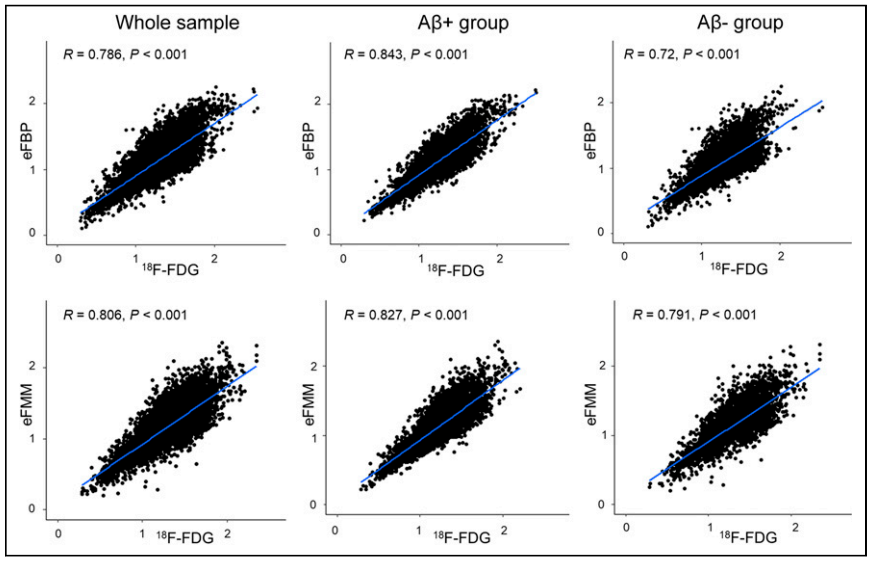

FIGURE 1. Correlation between eFBP/eFMM and ^{18}F-FDG PET SUVR. Scatterplots showing association between eFBP/eFMM SUVR (*y*-axis) in AAL regions and their respective ^{18}F-FDG SUVR (*x*-axis). Results are presented for whole sample and separately for subgroups divided according to Aβ status. Lines resulting from linear regression are shown in blue. *R* and *P* values are given in the upper left corner. FBP = florbetapir; FMM = flutemetamol; eFBP = early FBP; eFMM = early FMM; Aβ− = amyloid negative; Aβ+ = amyloid positive.

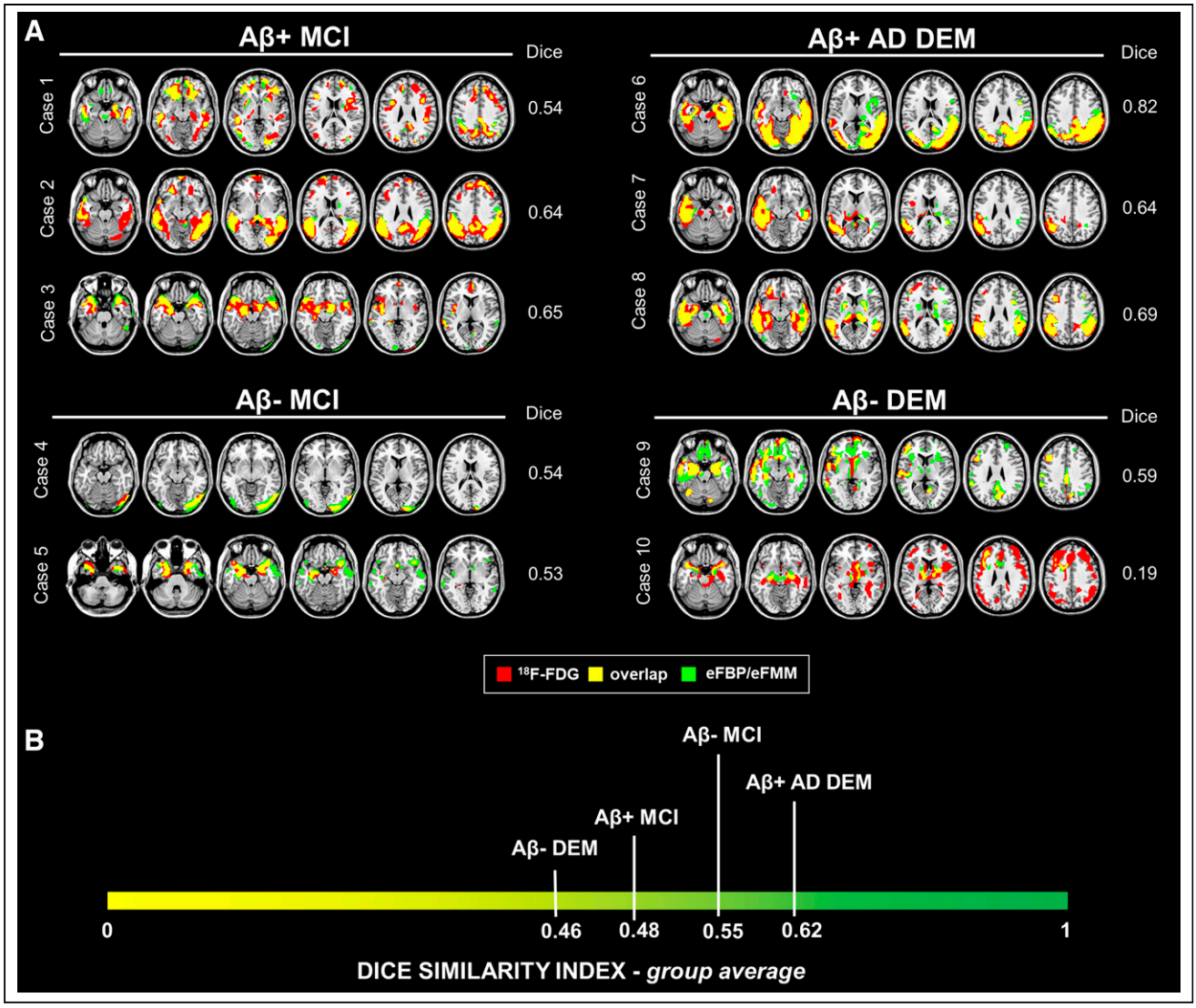

FIGURE 2. Hypometabolic and hypoperfusion patterns at the single-subject level. (A) Patterns of ^{18}F-FDG PET hypometabolism and eFBP/eFMM hypoperfusion in single individuals. Hypometabolism maps, hypoperfusion maps, and their overlap were imposed on standard Montreal Neurological Institute template. These maps were obtained from binarization of single-subject ^{18}F-FDG PET SPM T-maps and eFBP/eFMM SPM T-maps ($P < 0.05$ uncorrected, $k > 100$). The Dice similarity index is reported to the right of the brain template of each subject. (B) Clinical groups ordered according to degree of similarity between brain hypometabolism and hypoperfusion, as measured by Dice similarity index average. Lower-to-higher values of Dice indicate increasing degree of overlap. DEM = dementia; eFBP = early florbetapir; eFMM = early flutemetamol; Aβ+ = amyloid positive; Aβ− = amyloid negative; AD = Alzheimer disease; MCI = mild cognitive impairment.

TABLE 2

Contingency Table Reporting Frequency of Different Hypometabolism and Hypoperfusion Patterns in Whole Sample

	Hypoperfusion pattern						
Hypometabolism pattern	AD-like	FTD-like	DLB-like	Limbic-like	Unclassified	Normal	Total
AD-like	30	1	0	4	2	2	39
FTD-like	0	9	0	1	0	0	10
DLB-like	0	0	3	0	0	0	3
Limbic-like	0	0	0	14	0	0	14
Unclassified	0	0	0	1	24	1	26
Normal	2	0	0	0	1	29	32
Total	32	11	2	19	28	32	124

AD = Alzheimer disease; FTD = frontotemporal dementia; DLB = dementia with Lewy bodies.

TABLE 3

Distribution of Hypometabolism Patterns and Their Voxel-by-Voxel Concordance with Hypoperfusion Maps in Clinical Groups

^{18}F-FDG hypometabolism pattern	Dementia			MCI			CU			Whole group		
	Sample (n = 21)	Dice*	% visual match	Sample (n = 73)	Dice*	% visual match	Sample (n = 30)	Dice*	% visual match	Sample (n = 124)	Dice	% visual match
AD-like	10 (all Aβ+)	0.632 ± 0.159	90	25 (all Aβ+)	0.459 ± 0.178	68	4 (all Aβ+)	0.611 ± 0.135	100	39 (all Aβ+)	0.516 ± 0.185	77
FTD-like	5 (3 Aβ+, 2 Aβ−)	0.483 ± 0.201	80	5 (3 Aβ+, 2 Aβ−)	0.531 ± 0.128	100	0			10 (6 Aβ+, 4 Aβ−)	0.507 ± 0.161	90
DLB-like	0			3 (2 Aβ+, 1 Aβ−)	0.467 ± 0.236	100	0			3 (2 Aβ+, 1 Aβ−)	0.467 ± 0.236	100
Limbic-like	0			13 (9 Aβ+, 4 Aβ−)	0.504 ± 0.078	100	1 (all Aβ+)	0.521	100	14 (10 Aβ+, 4 Aβ−)	0.504 ± 0.075	100
Unclassified	6 (5 Aβ+, 1 Aβ−)	0.621 ± 0.071	83	13 (8 Aβ+, 5 Aβ−)	0.498 ± 0.205	100	7 (all Aβ+)	0.381 ± 0.293	86	26 (20 Aβ+, 6 Aβ−)	0.499 ± 0.217	92
Normal	0			14 (6 Aβ+, 8 Aβ−)		86†	18 (all Aβ+)		94†	32 (24 Aβ+, 8 Aβ−)		90†

*Average ± SD.
†Percentage of patients consistently negative on ^{18}F-FDG and early-phase scans.
FTD = frontotemporal dementia; DLB = dementia with Lewy bodies; MCI = mild cognitive impairment; CU = cognitively unimpaired; AD = Alzheimer disease.

present the results of visual analyses for the uptake distribution images. The visual rating of SPM maps allowed identification of 4 neurodegenerative patterns: temporoparietal hypometabolism (AD-like pattern, $n = 39$), temporoparietal and occipital hypometabolism (Lewy body (DLB)–like pattern, $n = 3$), frontotemporal hypometabolism (FTD-like pattern, $n = 10$), and limbic-like or medial–temporal pattern ($n = 14$). Thirty-two of 124 subjects showed negative ^{18}F-FDG scans for neurodegenerative patterns. Some subjects revealed severe atrophy on T1-weighted MRI and unclassifiable SPM patterns for neurodegenerative disease ($n = 26$). Despite this heterogeneity, for 86% of subjects the patterns identified by ^{18}F-FDG PET were consistently found in early-phase maps at visual assessment. The frequency of the different hypometabolism and hypoperfusion patterns classified on the basis of SPM map interpretation is reported in Table 2. Table 3 shows the frequency of hypometabolism patterns and their spatial overlaps with hypoperfusion maps as measured by Dice and visual assessment, in the whole sample and separately in the 3 clinical subgroups (CU, MCI, and dementia). The hypometabolic/hypoperfusion maps resulting in the 3 clinical subgroups are fully detailed in the supplemental materials.

Only 16 of 124 subjects (13%) showed a mismatch between ^{18}F-FDG and eFBP/eFMM scans. When we compared MRI total lesion volume and age-related white matter change scale scores between the matched and mismatched subgroups, we found a more severe cerebrovascular pathology in cases with mismatch than in matched cases (Mann–Whitney U = 384, $P = 0.021$, for total lesion volume; Mann–Whitney U = 431, $P = 0.041$, for age-related white matter change scale).

When we calculated Δ scores to explore discrepancies between the eFBP/eFMM and ^{18}F-FDG PET maps, the main difference was in the extent of the abnormalities. Sixty-five of 92 subjects showed positive Δ scores indicating that the hypometabolism patterns were more extended than the hypoperfusion ones (Δ scores, 13,012 ± 12,996 voxels), regardless of the clinical category. Only 27 of 92 subjects presented negative Δ scores, indicating hypoperfusion patterns slightly more extended than the hypometabolic ones (Δ scores, −6,606 ± 6,943 voxels).

Discriminative Performance of AD Meta-ROI Approach

When testing the performance of the eFBP/eFMM SUVR in the AD composite meta-ROI in distinguishing AD patients from HC subjects, we found good AUC discriminative values (eFBP AUC, 0.888, eFMM AUC, 0.801), like those of the ^{18}F-FDG SUVR (^{18}F-FDG AUC, 0.915 and 0.832, respectively). The DeLong test confirmed no significant differences in the discriminatory performance of different tracers (^{18}F-FDG vs. eFBP $P = 0.396$; ^{18}F-FDG vs. eFMM $P = 0.665$). Figure 3 compares the diagnostic performance of ^{18}F-FDG PET SUVR and eFBP/eFMM SUVR in the AD composite meta-ROI in terms of ROC curves for the whole AD-continuum group.

As for the other AD-related meta-ROIs (*37*), none presented significant differences in the discriminatory power of ^{18}F-FDG PET and eFBP/eFMM SUVR between AD patients and HC subjects (Supplemental Table 4).

DISCUSSION

This study compared early-phase amyloid PET with ^{18}F-FDG PET patterns and the power to discriminate subjects in the AD continuum and subjects with other neurodegenerative conditions from HC. The correlation between cerebral perfusion and metabolism

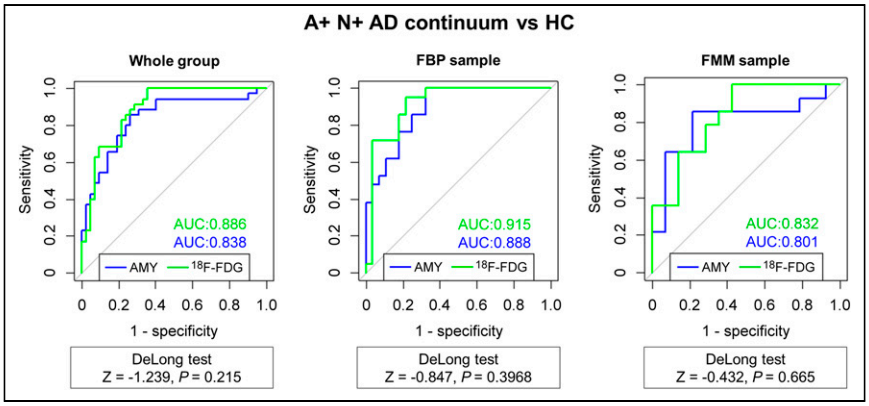

FIGURE 3. Discriminative performance of eFBP/eFMM and ^{18}F-FDG PET SUVR. ROC curves showing diagnostic performance of ^{18}F-FDG PET and eFBP/eFMM SUVR in AD composite meta-ROI for distinguishing AD patients from HC. AUCs for eFBP/eFMM and ^{18}F-FDG PET are shown in blue and green, respectively. Results of De Long test comparing 2 AUCs (eFBP/eFMM vs. ^{18}F-FDG PET) are given in bottom box. A+ = Aβ-positive; N+ = neurodegeneration-positive; AUC = area under the curve; FBP = florbetapir; FMM = flutemetamol; AD = Alzheimer disease; HC = healthy controls.

has long been established in aging and dementia conditions based on neurovascular coupling (*8*). At the same time, early-acquisition images of amyloid PET have been proposed as a topographic or functional biomarker reflecting cerebral perfusion (*6*).

Dual-phase amyloid PET may thus offer the advantage of—in a single procedure—acquiring information about amyloidosis and brain perfusion deficits reflecting neurodegeneration (*6*). Published work has focused on the relationship between brain perfusion and metabolism at a group level, but to our knowledge no studies have yet evaluated whether early-phase images might replace ^{18}F-FDG PET images in single individuals. This study evaluated brain hypoperfusion at the single-subject level and its comparability to respective brain hypometabolism, demonstrating a good correlation and a similar capacity in distinguishing patients from controls. In the presence of neurodegeneration assessed by ^{18}F-FDG PET, eFBP/eFMM single-subject analysis showed clusters of significant hypoperfusion, compared with controls, with good correspondence to the brain hypometabolism topography. The spatial overlap showed independence from underlying neurodegeneration topography, but with a more clear-cut correspondence in the dementia stages (Fig. 2).

In line with previous studies (*10–18*), our study confirmed strong positive correlations between eFBP/eFMM and ^{18}F-FDG SUVR ($R > 0.72$, $P < 0.001$) in a memory clinic cohort (Fig. 1). The correlation was independent of the used Aβ radiotracers and Aβ status, in agreement with other studies (*10,11,13,15*). Further supporting the comparability between the eFBP/eFMM and ^{18}F-FDG PET images, we found that lower Mini-Mental State Examination scores correlated significantly with decreases in both perfusion and metabolism measures (*10,12,13,16*).

When we applied the SPM single-subject analysis on eFBP/eFMM images, clusters of significant hypoperfusion were present in patients compared with controls, with good correspondence to the hypometabolism maps (Fig. 2; Table 2). As for negative scans, characterizing mostly the CU and MCI subgroups, the perfusion maps' ability was comparable to that of metabolism maps in excluding the presence of neurodegeneration for 90% of the negative scans. In the sample of CU subjects, we found 60% ^{18}F-FDG PET–negative scans, and for 94% of these, eFBP/eFMM images agreed on ruling out neurodegenerative patterns.

In MCI, eFBP/eFMM maps were able to identify patterns specific to neurodegenerative conditions for most cases, showing a moderate-to-good degree of overlap with hypometabolism patterns (Table 3). In most cases, hypometabolism SPM maps showed a greater extent than the hypoperfusion ones, although the disease-specific hallmark was detectable in both (Fig. 2). The lack of a full overlap here between perfusion and metabolism maps is likely because they measure different brain biological processes (*8,17*). Other reasonable explanations are the noisy feature of the initial frames and the nonuniform delivery of the tracer (*13*). However, although the early-phase image may be noisier, the similarity between the patterns is also striking in MCI conditions, supporting its use (Fig. 2). A negative ^{18}F-FDG PET scan in MCI was confirmed in 86% of eFBP/eFMM images. This is compatible with the absence of neurodegeneration in MCI, followed by a stable condition at follow-up (*45,46*).

In dementia conditions, the high comparability of hypoperfusion and hypometabolism maps suggests an increase in concordance with the advance of disease stages (Fig. 2B). Since hypoperfusion usually showed less extension than hypometabolism maps, a more severe underlying neurodegeneration may be necessary to reveal specific patterns that are instead detectable with ^{18}F-FDG PET. This finding suggests that ^{18}F-FDG PET might be more suitable for preclinical and prodromal stages. Further studies are needed to specifically address preclinical phases, such as subjective cognitive decline, based on larger samples and follow-up data.

We found only 13% of subjects with a mismatch between hypometabolism and hypoperfusion maps in the whole sample, mostly in the CU and MCI groups. In these cases, the eFBP/eFMM images were less sensitive in detecting the underlying neurodegeneration than ^{18}F-FDG PET. The risk of having false-negative findings with early-phase imaging warrants an additional ^{18}F-FDG PET exam when clinical suspicion of neurodegenerative conditions is high. The group of mismatch cases showed greater cerebrovascular lesion volumes on MRI than the match group. This result is consistent with the fact that both ^{18}F-FDG PET and eFBP/eFMM images can suffer from biases in the presence of severe atrophy or cerebral vascular disease (*8*). Thus, this limitation needs to be considered in the application and interpretation of SPM analysis both with ^{18}F-FDG PET and with early-phase imaging.

Finally, we found good diagnostic performance for the meta-ROI approach using perfusion measures (Fig. 3). Both eFBP and eFMM SUVR in the AD composite meta-ROI significantly discriminated AD patients from HC subjects. At ROC analyses, ^{18}F-FDG SUVR was slightly superior to perfusion measures in discriminating these subjects from controls, but without reaching the significance threshold for differences ($P > 0.05$) (Fig. 3).

As a limitation of our study, we acquired the early-phase images using published protocols (*20*); however, different early time frames for eFBP have also been proposed in the literature to achieve the best association with ^{18}F-FDG PET (*16,18*). We are aware of the relatively limited sample size of HC subjects included for comparisons; further studies will help to confirm the findings.

An appropriate normalization procedure and HC dataset are mandatory to achieve good performances in voxel-wise analyses, and methods for early-phase images are, in this respect, less mature than for ^{18}F-FDG PET (*47*).

CONCLUSION

To our knowledge, this was the first study to evaluate, at the single-subject level by applying voxel-based analysis, the classification performance of early-phase amyloid PET images. eFBP and eFMM imaging is able to identify different and typical neurodegenerative patterns or to exclude the presence of neurodegeneration. Dual-phase amyloid PET permits assessment of neurodegeneration and Aβ pathology with a single tracer injection and should be systematically implemented in routine clinical practice. In our opinion, when there is discrepancy between clinical and imaging results, mainly in the early phase of the disease, an additional ^{18}F-FDG PET exam is recommended.

DISCLOSURE

PET scans were performed within research projects funded by the Swiss National Science Foundation (SNSF, projects 320030_169876, 320030_185028, and 320030_182772), Horizon 2020 (project 667375), Human Brain Project, and the EU-EFPIA Innovative Medicines Initiatives 2 Joint Undertaking (IMI 2 JU; grants 115952 and 115736). This project was funded in part by grants from the Swiss National Science Foundation (SNF 3200B0-1161193 and SPUM 33CM30-124111) and an unrestricted grant from the Association pour la Recherche sur l'Alzheimer, Geneva, Switzerland. The Centre de la mémoire at Geneva University Hospital, collecting data with contributions from the Clinical Research Center (University Hospital and Faculty of Medicine, Geneva), is funded by private donors: Association Suisse pour la Recherche sur l'Alzheimer, Genève; Fondation Segré, Genève; Fondazione Agusta, Lugano; Race Against Dementia Foundation, London, UK; Fondation Child Care, Genève; Fondation Edmond J. Safra, Genève; Fondation Minkoff, Genève; McCall Macbain Foundation, Canada; Nicole et Renè Keller, Genève; Fondation AETAS, Genève; VELUX Foundation. Cecilia Boccalini was supported by an IBRO Exchange Fellowship. No other potential conflict of interest relevant to this article was reported.

KEY POINTS

QUESTION: Can we use early-phase amyloid PET scans instead of ^{18}F-FDG PET for individual classification?

PERTINENT FINDINGS: The single-subject procedure applied to early-phase amyloid PET provided typical neurodegenerative patterns in patients as compared with controls, especially in the advanced stage of the diseases. The topographic similarity between the hypoperfusion and hypometabolic patterns was striking, supporting their use for individual classification. Early-phase amyloid PET imaging can exclude the presence of neurodegeneration.

IMPLICATIONS FOR PATIENT CARE: Dual-phase amyloid PET permits assessment of neurodegeneration and Aβ pathology with a single tracer injection in 1 exam, and its implementation will be optimal in terms of costs, patient comfort, and radiation exposure.

REFERENCES

1. Villemagne VL, Barkhof F, Garibotto V, Landau SM, Nordberg A, van Berckel BNM. Molecular imaging approaches in dementia. *Radiology.* 2021;298:517–530.
2. Perani D, Caminiti SP, Carli G, Tondo G. PET neuroimaging in dementia conditions. In: Dierckx RAJO, Otte A, de Vries EFJ, van Waarde A, Leenders KL, eds. *PET and SPECT in Neurology.* Springer; 2020:211–282.
3. Cerami C, Della Rosa PA, Magnani G, et al. Brain metabolic maps in mild cognitive impairment predict heterogeneity of progression to dementia. *Neuroimage Clin.* 2014;7:187–194.
4. Ossenkoppele R, Prins ND, Pijnenburg YAL, et al. Impact of molecular imaging on the diagnostic process in a memory clinic. *Alzheimers Dement.* 2013;9:414–421.
5. Silverman DHS, Mosconi L, Ercoli L, Chen W, Small GW. Positron emission tomography scans obtained for the evaluation of cognitive dysfunction. *Semin Nucl Med.* 2008;38:251–261.
6. Valentina G, Silvia M, Marco P. Dual-phase amyloid PET: hitting two birds with one stone. *Eur J Nucl Med Mol Imaging.* 2016;43:1300–1303.
7. Gjedde A, Aanerud J, Braendgaard H, Rodell AB. Blood-brain transfer of Pittsburgh compound B in humans. *Front Aging Neurosci.* 2013;5:70.
8. Silverman DHS. Brain ^{18}F-FDG PET in the diagnosis of neurodegenerative dementias: comparison with perfusion SPECT and with clinical evaluations lacking nuclear imaging. *J Nucl Med.* 2004;45:594–607.
9. Jueptner M, Weiller C. Does measurement of regional cerebral blood flow reflect synaptic activity?—Implications for PET and fMRI. *Neuroimage.* 1995;2:148–156.
10. Tiepolt S, Hesse S, Patt M, et al. Early [^{18}F]florbetaben and [^{11}C]PiB PET images are a surrogate biomarker of neuronal injury in Alzheimer's disease. *Eur J Nucl Med Mol Imaging.* 2016;43:1700–1709.
11. Seiffert AP, Gómez-Grande A, Villarejo-Galende A, et al. High correlation of static first-minute-frame (FMF) PET imaging after18F-labeled amyloid tracer injection with [18F]FDG pet imaging. *Sensors (Basel).* 2021;21:1–14.
12. Meyer PT, Hellwig S, Amtage F, et al. Dual-biomarker imaging of regional cerebral amyloid load and neuronal activity in dementia with PET and ^{11}C-labeled Pittsburgh compound B. *J Nucl Med.* 2011;52:393–400.
13. Rostomian AH, Madison C, Rabinovici GD, Jagust WJ. Early ^{11}C-PIB frames and ^{18}F-FDG PET measures are comparable: a study validated in a cohort of AD and FTLD patients. *J Nucl Med.* 2011;52:173–179.
14. Rodriguez-Vieitez E, Leuzy A, Chiotis K, Saint-Aubert L, Wall A, Nordberg A. Comparability of [^{18}F]THK5317 and [^{11}C]PIB blood flow proxy images with [^{18}F]FDG positron emission tomography in Alzheimer's disease. *J Cereb Blood Flow Metab.* 2017;37:740–749.
15. Daerr S, Brendel M, Zach C, et al. Evaluation of early-phase [^{18}F]-florbetaben PET acquisition in clinical routine cases. *Neuroimage Clin.* 2016;14:77–86.
16. Ottoy J, Verhaeghe J, Niemantsverdriet E, et al. ^{18}F-FDG PET, the early phases and the delivery rate of ^{18}F-AV45 PET as proxies of cerebral blood flow in Alzheimer's disease: validation against ^{15}O-H2O PET. *Alzheimers Dement.* 2019;15:1172–1182.
17. Peretti DE, García DV, Reesink FE, et al. Relative cerebral flow from dynamic PIB scans as an alternative for FDG scans in Alzheimer's disease PET studies. *PLoS One.* 2019;14:e0211000.
18. Vanhoutte M, Landeau B, Sherif S, et al. Evaluation of the early-phase [^{18}F]AV45 PET as an optimal surrogate of [^{18}F]FDG PET in ageing and Alzheimer's clinical syndrome. *Neuroimage Clin.* 2021;31:102750.
19. Forsberg A, Engler H, Blomquist G, Långström B, Nordberg A. The use of PIB-PET as a dual pathological and functional biomarker in AD. *Biochim Biophys Acta.* 2012;1822:380–385.
20. Hsiao IT, Huang CC, Hsieh CJ, et al. Correlation of early-phase ^{18}F-florbetapir (AV-45/Amyvid) PET images to FDG images: preliminary studies. *Eur J Nucl Med Mol Imaging.* 2012;39:613–620.
21. Rodriguez-Vieitez E, Carter SF, Chiotis K, et al. Comparison of early-phase ^{11}C-deuterium-L-deprenyl and ^{11}C-Pittsburgh compound B PET for assessing brain perfusion in Alzheimer disease. *J Nucl Med.* 2016;57:1071–1077.
22. Montandon ML, Herrmann FR, Garibotto V, Rodriguez C, Haller S, Giannakopoulos P. Determinants of mesial temporal lobe volume loss in older individuals with preserved cognition: a longitudinal PET amyloid study. *Neurobiol Aging.* 2020;87:108–114.
23. Giannakopoulos P, Rodriguez C, Montandon ML, Garibotto V, Haller S, Herrmann FR. Less agreeable, better preserved? A PET amyloid and MRI study in a community-based cohort. *Neurobiol Aging.* 2020;89:24–31.
24. Zanchi D, Montandon ML, Sinanaj I, et al. Decreased fronto-parietal and increased default mode network activation is associated with subtle cognitive deficits in elderly controls. *Neurosignals.* 2017;25:127–138.
25. Dodich A, Mendes A, Assal F, et al. The A/T/N model applied through imaging biomarkers in a memory clinic. *Eur J Nucl Med Mol Imaging.* 2020;47:247–255.

26. Frisoni GB, Barkhof F, Altomare D, et al. AMYPAD diagnostic and patient management study: rationale and design. *Alzheimers Dement.* 2019;15:388–399.
27. Albert MS, DeKosky ST, Dickson D, et al. The diagnosis of mild cognitive impairment due to Alzheimer's disease: recommendations from the National Institute on Aging–Alzheimer's Association workgroups on diagnostic guidelines for Alzheimer's disease. *Alzheimers Dement.* 2011;7:270–279.
28. McKhann GM, Knopman DS, Chertkow H, et al. The diagnosis of dementia due to Alzheimer's disease: recommendations from the National Institute on Aging–Alzheimer's Association workgroups on diagnostic guidelines for Alzheimer's disease. *Alzheimers Dement.* 2011;7:263–269.
29. Ribaldi F, Chicherio C, Altomare D, et al. Brain connectivity and metacognition in persons with subjective cognitive decline (COSCODE): rationale and study design. *Alzheimers Res Ther.* 2021;13:105.
30. Jessen F, Amariglio RE, Buckley RF, et al. The characterisation of subjective cognitive decline. *Lancet Neurol.* 2020;19:271–278.
31. Schmidt P. *Bayesian Inference for Structured Additive Regression Models for Large-Scale Problems with Applications to Medical Imaging.* Dissertation [chapter 6.1]. LMU München; 2016.
32. Wahlund LO, Barkhof F, Fazekas F, et al. A new rating scale for age-related white matter changes applicable to MRI and CT. *Stroke.* 2001;32:1318–1322.
33. Guedj E, Varrone A, Boellaard R, et al. EANM procedure guidelines for brain PET imaging using [^{18}F]FDG, version 3. *Eur J Nucl Med Mol Imaging.* 2022;49:632–651.
34. Boellaard R, Delgado-Bolton R, Oyen WJG, et al. FDG PET/CT: EANM procedure guidelines for tumour imaging: version 2.0. *Eur J Nucl Med Mol Imaging.* 2015;42:328–354.
35. Schmitt J, Palleis C, Sauerbeck J, et al. Dual-phase β-amyloid PET captures neuronal injury and amyloidosis in corticobasal syndrome. *Front Aging Neurosci.* 2021; 13:661284.
36. Rolls ET, Huang CC, Lin CP, Feng J, Joliot M. Automated anatomical labelling atlas 3. *Neuroimage.* 2020;206:116189.
37. Landau SM, Harvey D, Madison CM, et al. Associations between cognitive, functional, and FDG-PET measures of decline in AD and MCI. *Neurobiol Aging.* 2011; 32:1207–1218.
38. Perani D, Anthony P, Rosa D, et al. Validation of an optimized SPM procedure for FDG-PET in dementia diagnosis in a clinical setting. *Neuroimage Clin.* 2014;6: 445–454.
39. Caminiti SP, Ballarini T, Sala A, et al. FDG-PET and CSF biomarker accuracy in prediction of conversion to different dementias in a large multicentre MCI cohort. *Neuroimage Clin.* 2018;18:167–177.
40. Tondo G, Carli G, Santangelo R, et al. Biomarker-based stability in limbic-predominant amnestic mild cognitive impairment. *Eur J Neurol.* 2021;28: 1123–1133.
41. Teune LK, Bartels AL, De Jong BM, et al. Typical cerebral metabolic patterns in neurodegenerative brain diseases. *Mov Disord.* 2010;25:2395–2404.
42. Jenkinson M, Beckmann CF, Behrens TEJ, Woolrich MW, Smith SM. FSL. *Neuroimage.* 2012;62:782–790.
43. Savio A, Fünger S, Tahmasian M, et al. Resting-state networks as simultaneously measured with functional MRI and PET. *J Nucl Med.* 2017;58:1314–1317.
44. DeLong ER, DeLong DM, Clarke-Pearson DL. Comparing the areas under two or more correlated receiver operating characteristic curves: a nonparametric approach. *Biometrics.* 1988;44:837–845.
45. Pandya SY, Clem MA, Silva LM, Woon FL. Does mild cognitive impairment always lead to dementia? A review. *J Neurol Sci.* 2016;369:57–62.
46. Petersen RC, Lopez O, Armstrong MJ, et al. Practice guideline update summary: mild cognitive impairment—report of the Guideline Development, Dissemination, and Implementation Subcommittee of the American Academy of Neurology. *Neurology.* 2018;90:126–135.
47. Della Rosa PA, Cerami C, Gallivanone F, et al. A standardized [^{18}F]-FDG-PET template for spatial normalization in statistical parametric mapping of dementia. *Neuroinformatics.* 2014;12:575–593.